The shape of the $T_z = +1$ Nucleus ^{94}Pd and the role of Proton-Neutron Interactions on the Structure of its Excited States

A. Yaneva[a,b], S. Jazrawi[c,d], M. Mikołajczuk[b,e], M. Górska[b], P. H. Regan[c,d], B. Das[b,f], H. M. Albers[b], S. Alhomaidhi[b,g,h,i], T. Arici[b], A. Banerjee[b], G. Benzoni[k], B. Cederwall[f], M. M. R. Chishti[c], D. D. Dao[j], T. Davinson[l], A. Gargano[m], J. Gerl[b], O. Hall[l], N. Hubbard[b,g,h], J. Jolie[a], I. Kojouharov[b], A. K. Mistry[b,h], F. Nowacki[j], M. Polettini[k,n,1,2], M. Rudigier[h], E. Şahin[b,g,h], H. Schaffner[b], A. Sharma[o], M. Armstrong[a,b], H. J. Wollersheim[b], P. Boutachkov[b], T. Dickel[b], E. Haettner[b], H. Heggen[b], Ch. Hornung[b], R. Knöbel[b], D. Kostyleva[b], N. Kurz[b], N. Kuzminchuk[b], I. Mukha[b], S. Pietri[b], W. R. Plass[b], Zs. Podolyák[c], C. Scheidenberger[b], Y. K. Tanaka[p], J. Vesic[q], H. Weick[b], U. Ahmed[g,h], Ö. Aktas[f], A. Algora[r,s], C. Appleton[l], J. Benito[t], A. Blazhev[a], A. Bracco[k,n], A. M. Bruce[u], M. Brunet[c], R. Canavan[c,d], A. Esmaylzadeh[a], L. M. Fraile[t], G. Häfner[a,v], K. P. Hucka[i], P. R. John[h], D. Kahl[l], V. Karayonchev[a,3], R. Kern[h], G. Košir[q,w], R. Lozeva[v], P. Napiralla[i], B. S. Nara Singh[x], R. Page[y], C. M. Petrache[22v], N. Pietralla[h], J.-M. Régis[a], H. Rösch[h], P. Ruotsalainen[z], V. Sanchez-Temble[t], L. Sexton[l], R. Shearman[d], M. Si[v], V. Werner[g,h], J. Wiederhold[h], K. Wimmer[b], W. Witt[h], P. Woods[l], G. Zimba[z]

[a] *Institut für Kernphysik der Universität zu Köln, D-50937 Köln, Germany*
[b] *GSI Helmholtzzentrum für Schwerionenforschung GmbH, Planckstr. 1, 64291 Darmstadt, Germany*
[c] *School of Mathematics and Physics, University of Surrey, Guildford, GU2 7XH, UK*
[d] *National Physical Laboratory, Teddington, Middlesex, TW11 0LW, UK*
[e] *Faculty of Physics, University of Warsaw, Warsaw 00681, Poland*
[f] *KTH Royal Institute of Technology, Stockholm, Sweden*
[g] *Helmholtz Forschungsakademie Hessen für FAIR (HFHF), GSI Helmholtzzentrum für Schwerionenforschung, Campus Darmstadt, 64289 Darmstadt-Arheilgen, Germany*
[h] *Institut für Kernphysik, Technische Universität Darmstadt, Darmstadt, Germany*
[i] *King Abdulaziz City for Science and Technology (KACST), P.O.Box 6086, Riyadh 11442, Saudi Arabia*
[j] *Université de Strasbourg, IPHC, 23 rue du Loess 67037 Strasbourg, France*
[k] *INFN, Sezione di Milano, Milano, Italy*
[l] *School of Physics and Astronomy, University of Edinburgh, Edinburgh H9 3FD, UK*
[m] *Istituto Nazionale di Fisica Nucleare, Complesso Universitario di Monte S. Angelo, I-80126 Napoli, Italy*
[n] *Dipartimento di Fisica, Universita degli Studi di Milano, Milano, Italy*
[o] *Department of Physics, Indian Institute of Technology Ropar, Rupnagar 140001, Punjab, India*
[p] *High-Energy Nuclear Physics Laboratory, RIKEN, 351-0198 Saitama, Japan*
[q] *Jozef Stefan Institute, Jamova cesta 39, 1000 Ljubljana, Slovenia*
[r] *Instituto de Fisica Corpuscular, CSIC-Universidad de Valencia, E-46071 Valencia, Spain*
[s] *Institute for Nuclear Research (ATOMKI), Bem ter 18/c, H-4026 Debrecen, Hungary*
[t] *Grupo de Física Nuclear and IPARCOS, Universidad Complutense de Madrid, CEI Moncloa, E-28040 Madrid, Spain*
[u] *School of Computing Engineering and Mathematics, University of Brighton, BN2 4AT Brighton, UK*
[v] *Université Paris-Saclay, IJCLab, CNRS/IN2P3, F-91405 Orsay, France*
[w] *Faculty of Mathematics and Physics, University of Ljubljana, Ljubljana, Slovenia*
[x] *School of Computing, Engineering and Physical Sciences, University of the West of Scotland, PA1 2BE Paisley, UK*
[y] *Department of Physics, Oliver Ladge Laboratory, University of Liverpool, Liverpool L69 7ZE, UK*
[z] *University of Jyväskylä, Seminaarinkatu 15, 40014 Jyväskylän yliopisto, Finland*

Abstract

Reduced transition probabilities have been extracted between excited, yrast states in the $N = Z + 2$ nucleus ^{94}Pd. The transitions of interest were observed following decays of the $I^{\pi} = 14^{+}$, $E_x = 2129$-keV isomeric state, which was populated following the projectile fragmentation of a ^{124}Xe primary beam at the GSI Helmholtzzentrum für Schwerionenforschung accelerator facility as part of FAIR Phase-0. Experimental information regarding the reduced E2 transition strengths for the decays of the yrast 8^{+} and 6^{+} states was determined following isomer-delayed $E_{\gamma 1} - E_{\gamma 2} - \triangle T_{2,1}$ coincidence method, using the $LaBr_3$(Ce)-based FATIMA fast-timing coincidence gamma-ray array, which allowed direct determination of lifetimes of states in ^{94}Pd using the Generalized Centroid Difference (GCD) method. The experimental value for the half-life of the yrast 8^{+} state of 755(106) ps results in a reduced transition probability of B(E2:$8^{+} \rightarrow 6^{+}$) = 205^{+34}_{-25} e^{2}fm^4, which enables a precise verification of shell-model calculations for this unique system, lying directly between the $N = Z$ line and the $N = 50$ neutron shell closure. The determined $B(E2)$ value provides an insight into the purity of $(g_{9/2})^n$ configurations in competition with admixtures from excitations between the (lower) $N = 3$ pf and (higher) $N = 4$ gds orbitals for the first time. The results indicate weak collectivity expected for near-zero quadrupole deformation and an increasing importance of the $T = 0$ proton-neutron interaction at $N = 48$.

Keywords: γ spectroscopy, Fast timing, *pn* interacion, Isovector vs. isoscalar pairing, Shell Model

1. Introduction

The $N = Z = 50$ ^{100}Sn is the heaviest self-conjugate doubly-magic nucleus that is stable with respect to particle emission. Nuclear structure of hole states in the region "south-west" of the shell closure between the $N = 50$, $Z = 40$ and the $N = Z$ lines is dominated by the $0g_{9/2}$ intruder orbital from the $N = 4$ harmonic oscillator shell. It is well separated from the $N = 3$ pf-shell orbitals, both energetically and by its parity, allowing only two-particle two-hole ($2p2h$) excitations into the intruder orbital. This first valence high-spin orbit requires an additional quantum label in its n-particle wave functions, namely the seniority ν, which counts the number of unpaired nucleons for protons and neutrons occupying the same shell-model orbital. Dominated by the strong proton-neutron (pn) interaction, the $0g_{9/2}$ orbital gives rise to unique structural features such as spin-gap, seniority and parity-change isomerism, as well as proton-neutron pairing and seniority-induced symmetries. Therefore, the region "south-west" of ^{100}Sn remains the subject of increasing focus for both experimental and theoretical investigation [1, 2].

Initially, limited valence-space shell-model studies were performed employing empirical interactions in the $\pi\nu(1p_{1/2}0g_{9/2})$ model space. They are reviewed in reference [1]. More recently, realistic interactions and Large Scale Shell Model (LSSM) calculations were presented for the full $\pi\nu(f_{5/2}pg_{9/2})$ [3] as well as the upper $\pi\nu(gds)$ shell using the Nowacki-Sieja interaction [4]. Remnants of the seniority level scheme in the open $\pi\nu(g_{9/2})$ orbitals have also been addressed in reference [5]. Experimental work on this topic includes the discovery of core-excited isomers in ^{98}Cd [6, 7] and ^{96}Ag [8]; the yrast spectroscopy of ^{92}Pd [9] and the decay of the $I^\pi = 16^+$ spin trap isomer and yrast sequence in ^{96}Cd [4, 10, 11]. The strength of the pn interaction in the $\pi\nu(g_{9/2})$ orbitals manifests itself best in the strongly-binding $T = 0$ $(g_{9/2})^2$, $I^\pi = 9^+$ isoscalar two-body matrix element (TBME), which is comparable with the $T = 1$ isovector pairing [12, 13].

Following the discovery of excited states in ^{92}Pd [9], a series of multi-step shell-model and Independent Boson Model (IBM) studies investigated the role of $\pi\nu(g_{9/2})$ proton-neutron pairs with maximum aligned spins of 9^+ in the $N = Z$ nuclei ^{96}Cd, ^{94}Ag and ^{92}Pd with particular interest on the dependence of the controlling 9^+-TBME [9, 14, 15, 16, 17]. The content of the various pn-pairs within the nuclear wave functions in the three nuclei with increasing spin was discussed. However, overlap of the aligned 9^+-pn-boson wave functions with the exact shell-model diagonalization could only be established for low- and high-spin states, and little overlap was found for intermediate spin [17]. These conclusions are subject to modifications when excitations in the full $\pi\nu(f_{5/2}pg_{9/2})$ and $\pi\nu(gds)$ space are considered.

In Ref. [18], predictions in these model spaces were compared with a pure $(g_{9/2})^n$ approach for $B(E2)$ values and spectroscopic quadrupole moments in ^{92}Pd and ^{96}Cd. In the low-spin range ($I \leq 6$), the three approaches are equivalent for excitation energy and $B(E2)$ values, but exhibit large differences in the (presently experimentally inaccessible) spectroscopic quadrupole moments. Moreover, the lower-Z nuclei in the $g_{9/2}$ orbital exhibit signs of significant quadrupole deformation [19]. This is expected to evolve for higher spins and for nuclei closer to the $N = Z = 50$ doubly-magic closure due to model space exhaustion, resulting in a gradual reduction in collectivity.

The $T_z = +1$ nucleus ^{94}Pd, with its 2 neutron and 4 proton holes in $g_{9/2}$ orbital below ^{100}Sn, is situated at a crucial point of this evolution. It is the neighbour of the even-even $N = Z$ systems ^{92}Pd and ^{96}Cd, and represents the $T = 1$ isospin partner for states in the odd-odd $N = Z$ system ^{94}Ag. In particular, the detailed structure of the 8^+ seniority remnant state in ^{94}Pd will reveal the interplay between the isovector and isoscalar coupling of the pn pairs. Moreover, the structure of ^{94}Pd in terms of seniority-mixed states may provide a first indication of emerging collectivity when nucleons are removed from the doubly-magic system ^{100}Sn. The emergence of deformation is also supported by the prediction that favoured pn $T = 0$ pairs arrange themselves in a spin-aligned configuration to form shears blades in the Anti-Magnetic Rotational (AMR) behaviour for the yrast band of ^{92}Pd [20]. A recent theoretical publication using the EXVAM (Excited VAMPIR) approach [21] notes the relation of $T = 0$ pn-pairing component to the emergence of prolate deformation and shape coexistence in ^{94}Pd.

The experimental information on excited states in ^{94}Pd is available up to spin-parity $I^\pi = (20^+)$ and originates from experiments in which decays of the isomeric states with spin-parity $I^\pi = 14^+$ and (19^-) were studied [22, 23, 24], and from high-spin β-decay studies of ^{94}Ag [25, 26]. Only states fed by delayed transitions are known and no prompt γ-ray radiation from states in ^{94}Pd has so far been observed.

This letter presents results on electromagnetic transition rates between yrast states in ^{94}Pd. This allows a direct comparison between the predictions of various approaches of shell-model interactions and valence spaces. Special interest is put on pn interaction treatment for this $T_z = +1$ nucleus intermediate between the $N = Z$ line and the $N = 50$ closed neutron shell.

2. Experimental details

The decay of the isomeric, yrast $I^\pi = 14^+$ state in ^{94}Pd [24] was studied through its production via the projectile fragmentation of a ^{124}Xe primary beam at 982 MeV/u from the SIS18 synchrotron at GSI Helmholtzzentrum für Schwerionenforschung accelerator facility, Darmstadt, Germany. The secondary cocktail beam, resulting from reactions between the primary beam and a 4 g/cm^2 thick ^{9}Be target, was separated in terms of mass-to-charge ratio (A/Q) and atomic number (Z) in the FRagment Separator (FRS) [27]. The fragmentation products were identified on an event-by-event basis using the standard $B\rho - \triangle E - B\rho$

Email addresses: a.yaneva@gsi.de (A. Yaneva), m.gorska@gsi.de (M. Górska)

[1]Present adress: Universitá degli Studi di Padova, Italy

[2]Present adress: INFN Sezione di Padova, Italy

[3]Present adress: Argonne National Laboratory, Argonne IL 60439, USA

and $ToF-B\rho-\triangle E$ identification methods [28]. The ions reaching the final focal plane of the FRS were implanted in the Advanced Implantation Detector Array (AIDA) [29] in the center of the DEcay SPECtroscopy (DESPEC) setup [30]. The γ rays emitted in the deexcitation of the 14^+ isomeric state ($T_{1/2}$ = 515(1) ns) in ^{94}Pd were registered using 6 triple-cluster High Purity Germanium (HPGe) detectors (GALILEO) [31, 32] and 36 $LaBr_3$(Ce) detectors, constituting the FAst TIMing Array (FATIMA) [33, 34]. Each detector subsystem was equipped with an independent data acquisition system. The synchronization of the different subsystems was achieved using White Rabbit (WR) time stamp [35], which is driven by a 125 MHz clock with time accuracy of up to $\sim$ 1 ns. A preliminary analysis of these data on excited states transition rates in ^{96}Pd has been reported by the collaboration [36].

3. Data analysis and results

To extract nuclear excited-state mean lifetimes, the energy and timing data recorded by the FATIMA array were used to construct $E_{\gamma_1} - E_{\gamma_2} - \triangle T_{2,1}$ coincidence cubes, where a delayed coincidence condition on implanted ^{94}Pd ions was applied. The γ-ray spectrum obtained as total projection of this matrix is shown in Fig. 1(a) along with a resulting coincidence spectrum with the 1092-keV γ ray in Fig. 1(b). A time alignment was performed for all FATIMA detectors using coincidences between the 344- and 779-keV transitions from ^{152}Eu source data. The centroid of the delayed time distribution [37, 38, 39]

$$C(D) = \frac{\int_{-\infty}^{\infty} tD(t)dt}{\int_{-\infty}^{\infty} D(t)dt} \tag{1}$$

was calculated for each detector pair. The centroid of the anti-delayed time distribution was obtained in an analogous way. The generalized centroid difference ($\triangle C$) was obtained by subtracting the two centroids. In the Generalized Centroid Difference (GCD) method [38, 39] $\triangle C$ is directly related to the mean lifetime τ according to the expression:

$$\triangle C(\triangle E_\gamma) = PRD(\triangle E_\gamma) + 2\tau, \tag{2}$$

where the symmetry condition with respect to feeder-decay inversion [37] is:

$$\begin{aligned} \triangle C(\triangle E_\gamma)_{decay} &= -\triangle C(-\triangle E_\gamma)_{feeder} \\ PRD(\triangle E_\gamma)_{decay} &= -PRD(-\triangle E_\gamma)_{feeder}. \end{aligned} \tag{3}$$

Here $\triangle E_\gamma = E_{feeder} - E_{decay}$ is the energy difference between the feeding and decaying γ rays and $PRD(\triangle E_\gamma) = PRD(E_{feeder}) - PRD(E_{decay})$ is the prompt response difference. The PRD is energy dependent and was calibrated using various coincident transitions from ^{152}Eu source data. The values were adjusted to the 344-keV reference energy and fitted using the equation [38]:

$$PRD(E_\gamma) = \frac{a}{\sqrt{E_\gamma + b}} + cE_\gamma + d, \tag{4}$$

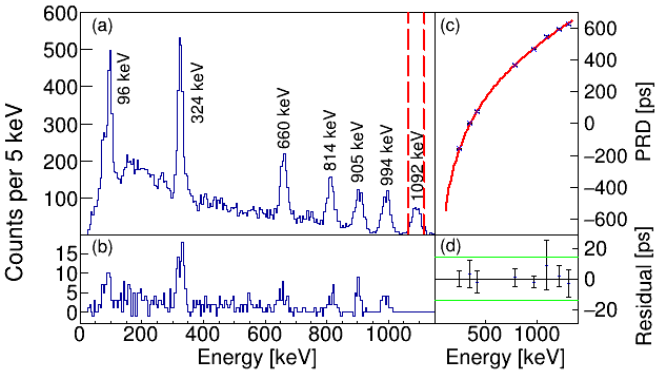

Figure 1: (a) Total projection of $\gamma-\gamma$ matrix for isomer-delayed γ rays obtained from FATIMA and correlated to implantation of ^{94}Pd ions. The matrix includes γ rays registered within 5 ns from each other. (b) Background-subtracted energy spectrum of γ rays measured in coincidence with the 1092-keV transition, as marked by the dashed red lines in (a). (c) PRD calibration and (d) residuals for the PRD fit.

where a, b, c, d are the parameters for the fit presented in Fig. 1(c). The fit residuals in Fig. 1(d) allow the systematic error of the PRD to be evaluated.

This analysis method is sufficiently accurate to measure excited-state half-lives in the range from of tens of picoseconds to nanoseconds, therefore a careful background treatment is essential. To minimize the influence of the Compton background underneath the full-energy peaks (FEP), the experimental centroid difference $\triangle C_{exp}$ was corrected using [40]:

$$\triangle C_{FEP} = \triangle C_{exp} + \frac{t_{corr}(decay) + t_{corr}(feeder)}{2} \tag{5}$$

$$t_{corr} = \frac{\triangle C_{exp} - \triangle C_{BG}}{P/B}, \tag{6}$$

where $\triangle C_{BG}$ is the centroid difference of the background time distribution, obtained for peak-background coincidences for both the decay and the feeding transition background, and P/B is the peak-to-background ratio. The $\triangle C_{FEP}$ values derived in this way along with the PRD values for the feeder-decay energy combinations obtained from the PRD curve were used in Eq.(2) to calculate the final mean lifetimes.

To determine the half-lives of the yrast $I^\pi = 6^+$ and 8^+ states in ^{94}Pd, the direct and indirect feeder-decay coincidences were used to produce delayed and anti-delayed time distributions. Direct coincidence in this work refers to the coincidences between the direct feeder and the direct decay transitions of a particular state. Indirect coincidences are considered when at least one of the feeder and decay transitions are not directly populating or deexciting the state of interest. However, the use of indirect coincidences for intrinsic state half-life measurements in ^{94}Pd is only possible assuming a prompt decay of the $I^\pi = 2^+$, 4^+, 10^+ and 12^+ states with respect to the state under investigation. In the present work it was assumed that the lifetimes of other states were shorter than 20 ps.

To determine the half-life of the $I^\pi = 6^+$, the direct coincidence between the 324- and 660-keV transitions, as well as indirect coincidences between the 324- and 905-keV, and 324-

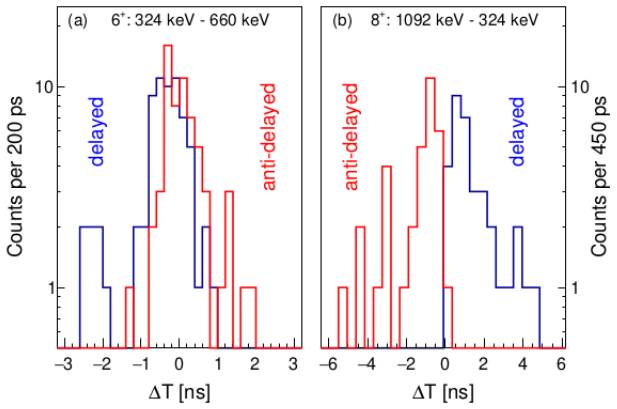

Figure 2: Delayed and anti-delayed time distributions for coincidences between the (a) 324- and 660-keV, as well as the (b) 1092- and 324-keV transitions in ^{94}Pd.

and 814-keV transitions ware used. Similarly, for the half-life of the yrast $I^\pi = 8^+$ state coincidences between the direct 1092- and 324-keV transitions was used in the first instance. In view of its long lifetime, the half-life of this state was determined also using the indirect coincidences between the transitions 1092 and 660 keV, 994 and 324 keV, 994 and 660 keV, 994 and 905 keV, 96 and 324 keV, 96 and 660 keV, 96 and 905 keV, 96 and 814 keV. For each coincidence, the delayed and anti-delayed time difference distributions were produced and their centroids determined. As an example, the time distributions of the direct coincidences for the 6^+ and 8^+ states in ^{94}Pd are shown in Fig. 2(a) and (b), respectively. After treating the background according to the procedure explained above, and accounting for the PRD shift correction for the particular coincidence, the mean-lifetime (τ) and half-life ($T_{1/2} = \tau ln2$) of the state of interest were obtained according to Eq.(2).

The experimentally-derived half-life for the $I^\pi = 6^+$ yrast state at $E_x = 2379$ keV was obtained from a weighted average of all determined excited-state half-lives (both from direct and indirect feeder-decay coincidences), resulting in the limit of $T_{1/2}(6^+) \leq 50$ ps. The analysis of the coincidence between the direct feeder-decay transitions of the $I^\pi = 8^+$ state at $E_x = 2703$ keV yields a half-life value of 755(106) ps. The weighted average of individually measured half-lives for indirect coincidences resulted in the value of $T_{1/2} = 825(50)$ ps, which corresponds to the effective values with embedded half-lives of intermediate states.

4. Discussion

The experimental results presented in this work are discussed within the shell-model framework. In Fig. 3 the experimentally-established level energies together with the known γ rays are shown in comparison to the two most advanced shell-model calculations in the full diagonalization of the nuclear Hamiltonian. The first one uses the JUN45 interaction [3] in the full $\pi\nu(f_{5/2}pg_{9/2})$ model space, while the second one is a LSSM calculation employing the GDS interaction [4] with $\pi\nu(gds)$ as the model space. Both calculations reproduce the experimental

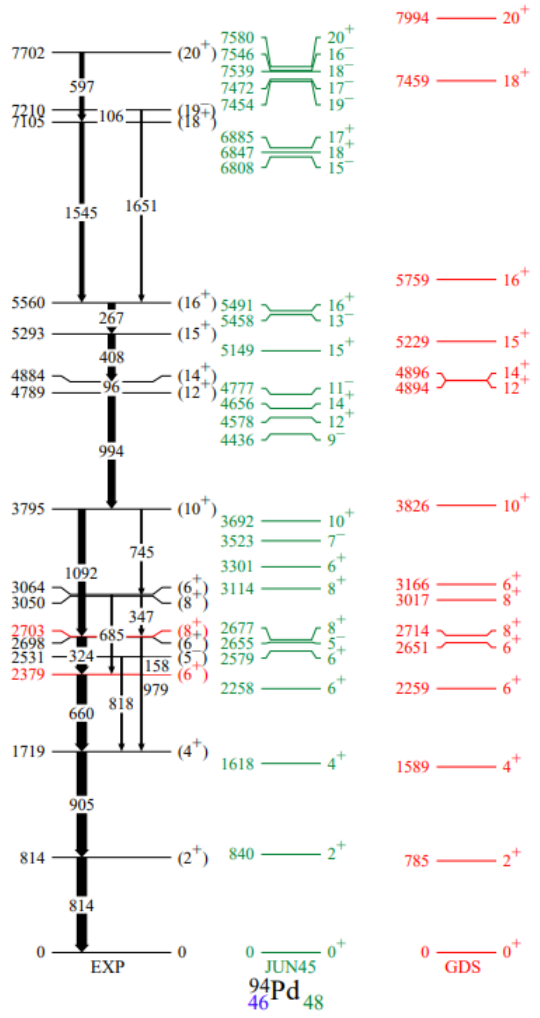

Figure 3: Experimental level scheme of excited states in ^{94}Pd [22, 23, 24, 25, 26] as well as shell-model calculations, employing the JUN45 [3] and GDS [4] interactions (see text for details).

yrast level energies very well up to the highest known spins.

In order to access the structure of involved states, and the associated nuclear deformation using the $\pi\nu(gds)$ valence space and effective GDS Hamiltonian, the potential energy surface (PES) of ^{92,94,96}Pd were obtained from Discrete Nonorthogonal Shell Model (DNO-SM) calculations in the same way as introduced in Ref. [41, 42]. As shown in Fig 4, ^{94}Pd exhibits a non-spherical shallow minimum at moderate prolate deformation. The ground-state wave function contains dominant contributions around $\beta \sim 0.1-0.2$ to high spins for the yrast and yrare states with no other coexisting minimum found in the PES. This is at variance with the claim made in Ref. [21]. The predicted (β, γ) distributions in the wave functions evolve from a spherical regime in ^{96}Pd towards a more axially-deformed prolate shape in the $N = Z$ system ^{92}Pd (see Fig. 4), with $T_z = +1$ ^{94}Pd being the transitional nucleus between these two extremes. This trend is particularly noticeable in the $I^\pi = 0^+$ ground states. For the $I^\pi = 8^+$ state in ^{96}Pd the shape remains spherical, whereas the deformation pattern in the two other nuclei shifts towards

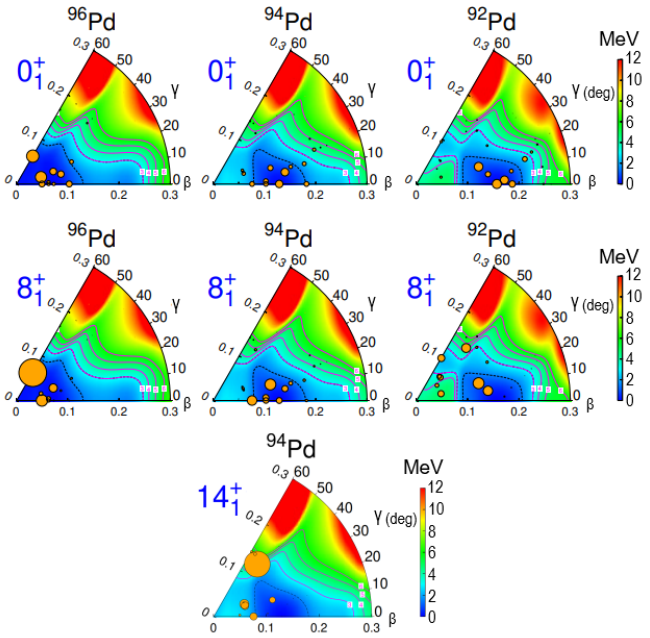

Figure 4: Potential energy surface (PES) plots for ^{96,94,92}Pd nuclei for the ground state as well as for the first $I^\pi = 8^+$ states. Additionally, the PES for the $I^\pi = 14^+$ state in ^{94}Pd is shown indicating a shallow prolate minimum (see text for details).

sphericity and maintains as such up to higher spins, in particular for the 14^+ state in ^{94}Pd. It should be noted that in ^{92}Pd, where the development of an axial prolate shape in the ground state is the most pronounced, there is no indication of other shape-coexisting minima within the configuration space.

The experimentally-obtained half-lives for the 6^+ and 8^+ states in ^{94}Pd from the current work were used to determine reduced $E2$ transition strengths. The deduced $B(E2)$ values, together with the value for the decay of the $I^\pi = 14^+$ isomeric state reported in Ref. [43], are summarized and compared to the two aforementioned shell-model approaches (JUN45, GDS) in Table 1 and Fig. 5. The values from Ref. [21] are provided in the table for a cross comparison. Effective charges of $e_\pi = 1.8e$ and $e_\nu = 0.8e$ according to Ref. [3, 44] were used for the JUN45 interaction [3] in Table 1. This well-known realistic interaction, which has reproduced many nuclear properties from the $N = 3$ harmonic oscillator shell and the region of ^{56}Ni approaching ^{100}Sn, is based on the Bonn-C potential. The calculated $B(E2)$ values are largely overestimated when compared to the experimental data (see Fig. 5), which is most probably a consequence of the strong mixing of the upper fp shell with the $g_{9/2}$ orbital, characteristic for this interaction and required for lighter nuclei to substitute the missing $f_{7/2}$ orbital in the corresponding model space. Reducing the effective charges to $e_\pi = 1.5e$ and $e_\nu = 0.5e$ results in a better agreement for ^{94}Pd. However, even this modification does not allow a simultaneous reproduction of the 8^+ and the 14^+ states in view of the small experimental uncertainties.

The agreement between the experimental results and the most challenging LSSM calculation, which employs the GDS interaction [4], is excellent. The involvement of core excitations (up to 5p5h) in the $\pi\nu(gds)$ model space, with effective charges of $e_\pi = 1.1e$ and $e_\nu = 0.84e$ [45], exhibits an almost exact reproduction of high-spin states (see Fig. 3) as well as of the reduced transition rates (see Fig. 5).

Table 1: Experimental half-lives expressed in ns and $B(E2)$ strengths in e^2fm^4 for excited states in ^{94}Pd compared to various shell-model approaches. The experimental half-life value for the yrast $I^\pi = 14^+$ state is taken from Ref. [43].

Quantity [ns/e^2fm^4]	$I_i^\pi - I_f^\pi$		
	$14^+ \rightarrow 12^+$	$8^+ \rightarrow 6^+$	$6^+ \rightarrow 4^+$
$T_{1/2}$	515(1)	0.755(106)	≤0.05
$B_{exp}(E2)$	52.1(1)	205^{+34}_{-25}	≥90
$B_{JUN45}(E2)$	113	277	496
$B_{GDS}(E2)$	49	192	548
$B_{g_{9/2}}(E2)$	85	115	307
$B_{g_{9/2}T=0(pn)}(E2)$	63	152	308
$B_{g_{9/2}T=1(pn)}(E2)$	3	12	8
$B_{EXVAM}(E2)$[21]	56	165	336

On the other hand, the AMR calculations shown in Fig. 5 (denoted by solid line) reproduce the transition rates measured in the current work very well. Ref. [20] demonstrates a good reproduction of the energy levels in ^{92}Pd using the AMR coupling scheme. For ^{94}Pd, the calculation is based on a similar 4 quasiparticle configuration as for the ground state of ^{92}Pd, where the shears closing behaviour takes over beyond $I^\pi = 8^+$. This may indicate that the $T = 1$ proton-proton and neutron-neutron pairs in the $g_{9/2}$ orbitals rearrange themselves to form two oppositely aligned $T = 0$ pn shears blades, the closing mechanism of which takes over in generating the higher-spin states of ^{94}Pd and continues until the shears blades are maximally aligned at $I^\pi = 16^+$. This supports the dominance of the isoscalar ($T = 0$) phase beyond $I^\pi = 8^+$, as predicted by the shell-model calculations in the $g_{9/2}$ model space (Table. 1). It is worth noting that the 4 quasiparticle AMR configuration for the spin states $I^\pi < 8^+$ (denoted by dotted line in Fig. 5) is expected to mix with those of 2 quasiparticle one.

With the aim of examining further the interplay of the isoscalar ($T = 0$) versus isovector ($T = 1$) components of the pn shell-model interaction on the structure of ^{94}Pd, the excited-state lifetimes were analysed within the single-$0g_{9/2}$ model. Although shell-model results presented in the current work indicate that a multi-orbital space including cross shell $N, Z = 50$ excitations are needed to describe ^{94}Pd quantitatively, the restriction to this rather simple model is justified by the spherical or slightly-deformed nature of Pd nuclei evidenced by these results as well as by the prominent role played by the $0g_{9/2}$ orbital in the low-lying states of nuclei around $N, Z = 50$ [4, 9, 14, 15, 16]. Indeed, the wave-function overlap of all ^{94}Pd states with the $(\pi 0g_{9/2})^4 \otimes (\nu 0g_{9/2})^2$ configuration, as calculated within the LSSM approach, exceeds 95%. Calculations were performed by using the two-body effective interaction derived within the framework of the many-body perturbation theory

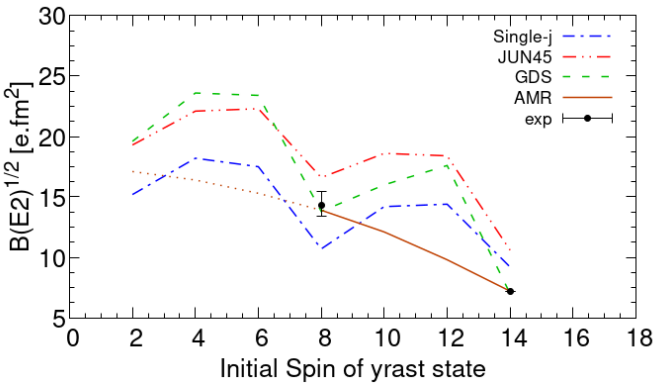

Figure 5: Experimental and shell-model calculated B(E2)$^{1/2}$ values, using different effective interactions and model spaces, for states in ^{94}Pd (see text for details).

starting from the high-precision CD-Bonn NN potential [46], as described in Ref. [47], where the list of the matrix elements is reported. In addition, two sets of interactions were obtained by separately removing the $T = 0$ and $T = 1$ pn matrix elements.

Similar to the $N = Z$ case of ^{92}Pd discussed in [47], the energies of the yrast levels of ^{94}Pd are reasonably-well reproduced when using the full interaction. A spectrum with the same structure is obtained only if the pure $T = 0$ pn component is considered, while the inclusion of only the $T = 1$ component leads to excited states compressed in a smaller energy interval, although the effect is smaller than the $N = Z$ system ^{92}Pd. These findings are in line with those reported in Ref. [9, 1], indicating that the evolution from the seniority to vibrational-type spectrum from ^{96}Pd to ^{92}Pd, with ^{94}Pd exhibiting an intermediate character is related to the $T = 0$ pn interaction.

This is the first time when such an analysis has been performed for $B(E2)$ transition strengths. Considering the significant restrictions of using a single-j space, standard values of the effective charges $e_\pi = 1.5e$ and $e_\nu = 0.5e$ were used. These serve only to investigate the relevance of the isovector with respect the isoscalar component of the pn interaction as shown in Table. 1. The results of the full interaction are shown in Fig. 5. The overall behavior is similar to that predicted by the JUN45 as well as the LSSM (GDS) approaches. However, the precision of the LSSM calculation when compared to the experimental values provides the best match, indicating again the relevance of core excitations. Furthermore, as shown in Table 1, the exclusion of the $T = 1 pn$ component from the single-j interaction do not vary significantly between the calculated B(E2) values with respect to the full interaction for the decay of the yrast $I_\pi = 6^+, 8^+$ and 14^+ states. In contrast, when considering a pure $T = 1$ force, considerably longer predicted half-lives are obtained. This finding demonstrates the effect of the different structure of the wave functions resulting from the $T = 1$ force, which is in general unable to produce a sufficient fragmentation of the basis states arising from the $(\pi 0g_{9/2})^4 \otimes (\nu 0g_{9/2})^2$ configuration.

5. Conclusion

The half-life and transitions rates for decays of intermediate-spin states in ^{94}Pd have been established using the FATIMA array. A range of restricted-basis model spaces and interactions were used to reproduce level energies and experimentally deduce $B(E2)$ values. The LSSM approach with a $\pi\nu(gds)$ model space provides the best agreement with the experimental results. This model indicates no development of deformation for Pd isotopes, which is predicted at the $N = Z$ line following a parallel potential energy surface analysis. Based on this conclusion, the $T = 0$ contribution of the pn interaction is manifested as the dominant one in the transition strengths of the 8^+ seniority remnant state and the 14^+ isomeric state.

Acknowledgements

The authors thank A. O. Macchiavelli for a valuable discussion. The authors would like to thank the staff of the FRS and the GSI accelerator, for their excellent support. The results were obtained in the context of FAIR Phase-0 Darmstadt, Germany. This work was supported by the Swedish Research Council under Grants No. 621-2014-5558 and No. 2019-04880. Support by the STFC under Grants No. ST/G000697/1, No. ST/P005314, and No. ST/P003982/1 and No. ST/P004598/1 and No. ST/V001027/1; by the UK Department for Business, Energy and Industrial Strategy via the National Measurement Office; by the BMBF under Grants No. 05P19RDFN1, No. 05P21RDFN1 and No. 05P21RDFN9; by the Helmholtz Research Academy Hesse for FAIR (HFHF); by the GSI F&E Grant No. KJOLIE1820; and by BMBF grant 05P19PKFNA and 0P21PKFN1 are also acknowledged. This work was supported by the Slovenian Research and Innovation Agency under Grants No. I0-E005 and No. P1-0102. P.H.R. and R.S. acknowledge support from the National Measurement System program unit of the UK's Department for BGS. G.H, M.S, and R.L. acknowledge IN2P3-GSI agreements, ADI-IDEX, and CSC-UPS grants. L.M.F. acknowledges the Spanish MICINN via Project No. RTI2018-098868-B-100. A.A. acknowledges partial support of the Ministerio de Ciencia e Innovacion Grant No. PID2019-104714GB-C21.

References

[1] T. Faestermann, M. Górska, H. Grawe, The structure of ^{100}Sn and neighbouring nuclei, Prog. Part. Nucl. Phys. 69 (2013) 85–130. doi:https://doi.org/10.1016/j.ppnp.2012.10.002.

[2] M. Górska, Trends in the Structure of Nuclei near ^{100}Sn, Physics 4 (2022) 364–382. doi:https://doi.org/10.3390/physics4010024.

[3] M. Honma, T. Otsuka, T. Mizusaki, M. Hjorth-Jensen, New effective interaction for f_5pg_9-shell nuclei, Phys. Rev. C 80 (2009) 064323. doi:https://doi.org/10.1103/PhysRevC.80.064323.

[4] B. S. Nara Singh, et al., 16^+ Spin-Gap Isomer in ^{96}Cd, Phys. Rev. Lett. 107 (2011) 172502. doi:https://doi.org/10.1103/PhysRevLett.107.172502.

[5] L. Zamick, Gaps in nuclear spectra as traces of seniority changes in systems of both neutrons and protons, Phys. Rev. C 93 (2016) 034327. doi:https://doi.org/10.1103/PhysRevC.93.034327.

[6] A. Blazhev, et al., Observation of a core-excited $E4$ isomer in ^{98}Cd, Phys. Rev. C 69 (2004) 064304. doi:https://doi.org/10.1103/PhysRevC.69.064304.

[7] A. Blazhev, et al., High-energy excited states in ^{98}Cd, J. Phys.: Conf. Ser. 205 (1) (2010) 012035. doi:https://doi.org/10.1088/1742-6596/205/1/012035.

[8] P. Boutachkov, et al., High-spin isomers in ^{96}Ag: Excitations across the $Z = 38$ and $Z = 50$, $N = 50$ closed shells, Phys. Rev. C 84 (2011) 044311. doi:https://doi.org/10.1103/PhysRevC.84.044311.

[9] B. Cederwall, et al., Evidence for a spin-aligned neutron–proton paired phase from the level structure of ^{92}Pd, Nature (London)) 469 (2011) 68–71. doi:https://doi.org/10.1038/nature09644.

[10] P. J. Davies, et al., The role of core excitations in the structure and decay of the 16^+ spin-gap isomer in ^{96}Cd, Phys. Lett. B 767 (2017) 474–479. doi:https://doi.org/10.1016/j.physletb.2017.02.013.

[11] P. J. Davies, et al., Toward the limit of nuclear binding on the N = Z line: Spectroscopy of ^{96}Cd, Phys. Rev. C 99 (2019) 021302(R). doi:https://doi.org/10.1103/PhysRevC.99.021302.

[12] F. J. D. Serduke, R. D. Lawson, D. H. Gloeckner, Shell-model study of the $N = 49$ isotones, Nucl. Phys. A 256 (1976) 45–86. doi:https://doi.org/10.1016/0375-9474(76)90094-4.

[13] R. L. Gross, A. Frenkel, Effective interaction of protons and neutrons in the $2p_{1/2}$-$1g_{9/2}$ subshells, Nucl. Phys. A 267 (1976) 85–108. doi:https://doi.org/10.1016/0375-9474(76)90645-X.

[14] S. Zerguine, P. Van Isacker, Spin-aligned neutron-proton pairs in $N = Z$ nuclei, Phys. Rev. C 83 (2011) 064314. doi:https://doi.org/10.1103/PhysRevC.83.064314.

[15] Z. X. Xu, C. Qi, J. Blomqvist, R. J. Liotta, R. Wyss, Multistep shell model description of spin-aligned neutron-proton pair coupling, Nucl. Phys. A 877 (2012) 51–58. doi:https://doi.org/10.1016/j.nuclphysa.2011.12.005.

[16] C. Qi, J. Blomqvist, T. Bäck, B. Cederwall, A. Johnson, R. J. Liotta, R. Wyss, Spin-aligned neutron-proton pair mode in atomic nuclei, Phys. Rev. C 84 (2011) 021301. doi:https://doi.org/10.1103/PhysRevC.84.021301.

[17] P. Van Isacker, Neutron-proton pairs in nuclei, Int. Journal Mod. Phys. E 22 (2013) 1330028. doi:https://doi.org/10.1142/S0218301313300282.

[18] A. P. Zuker, A. Poves, F. Nowacki, S. M. Lenzi, Nilsson-SU3 self-consistency in heavy $N = Z$ nuclei, Phys. Rev. C 92 (2015) 024320. doi:https://doi.org/10.1103/PhysRevC.92.024320.

[19] B. Cederwall, et al., Isospin Properties of Nuclear Pair Correlations from the Level Structure of the Self-Conjugate Nucleus ^{88}Ru, Phys. Rev. Lett. 124 (2020) 062501. doi:https://doi.org/10.1103/PhysRevLett.124.062501.

[20] S. Frauendorf, A. O. Macchiavelli, Overview of neutron-proton pairing, Prog. Part. Nucl. Phys. 78 (2014) 24–90. doi:https://doi.org/10.1016/j.ppnp.2014.07.001.

[21] A. S. Mare, A. Petrovici, Shape coexistence and isomeric states in ^{94}Pd within a beyond-mean-field approach, Phys. Rev. C 106 (2022) 054306. doi:https://doi.org/10.1103/PhysRevC.106.054306.

[22] M. Górska, et al., Proton-neutron interaction at $N \cong Z$ — First observation of the $T_z = 1$ nucleus $^{94}_{46}Pd_{48}$ in-beam, Z. Phys., A At. nucl. 353 (1995) 233–234. doi:https://doi.org/10.1007/BF01292324.

[23] R. Grzywacz, et al., New μs isomers in T_z=1 nuclei produced in the ^{112}Sn(63A MeV)+$^{\mathbf{nat}}$Ni reaction, Phys. Rev. C 55 (1997) 1126–1129. doi:https://doi.org/10.1103/PhysRevC.55.1126.

[24] T. S. Brock, others (RISING Collaboration), Observation of a new high-spin isomer in ^{94}Pd, Phys. Rev. C 82 (2010) 061309. doi:https://doi.org/10.1103/PhysRevC.82.061309.

[25] M. La Commara, et al., Beta decay of medium and high spin isomers in ^{94}Ag, Nucl. Phys. A 708 (2002) 167–180. doi:https://doi.org/10.1016/S0375-9474(02)01024-2.

[26] C. Plettner, et al., On the β-decaying (21^+) spin gap isomer in ^{94}Ag, Nucl. Phys. A 733 (2004) 20–36. doi:https://doi.org/10.1016/j.nuclphysa.2003.12.014.

[27] H. Geissel, et al., The GSI projectile fragment separator (FRS): a versatile magnetic system for relativistic heavy ions, Nucl. Instrum. Methods Phys. Res. B 70 (1992) 286–297. doi:https://doi.org/10.1016/0168-583X(92)95944-M.

[28] G. Münzenberg, The separation techniques for secondary beams, Nucl. Instrum. Methods Phys. Res. B 70 (1992) 265–275. doi:https://doi.org/10.1016/0168-583X(92)95942-K.

[29] O. Hall, et al., The Advanced Implantation Detector Array (AIDA), Nucl. Instrum. Methods Phys. Res. A 1050 (2023) 168166. doi:https://doi.org/10.1016/j.nima.2023.168166.

[30] A. K. Mistry, et al., The DESPEC setup for GSI and FAIR, Nucl. Instrum. Methods Phys. Res. A 1033 (2022) 166662. doi:https://doi.org/10.1016/j.nima.2022.166662.

[31] A. Goasduff, et al., The GALILEO γ-ray array at the Legnaro National Laboratories, Nucl. Instrum. Methods Phys. Res. A 1015 (2021) 165753. doi:https://doi.org/10.1016/j.nima.2021.165753.

[32] P. R. John, et al., Assembly of 8 Galileo TC at Institut für Kernphysik TU Darmstadt for the DESPEC Campaign (2020).

[33] M. Rudigier, et al., FATIMA - FAst TIMing Array for DESPEC at FAIR, Nucl. Instrum. Methods Phys. Res. A 969 (2020) 163967. doi:https://doi.org/10.1016/j.nima.2020.163967.

[34] M. M. R. Chishti, et al., Response of the FAst TIMing Array (FATIMA) for DESPEC at FAIR Phase-0, Nucl. Instrum. Methods A 1056 (2023) 168597. doi:https://doi.org/10.1016/j.nima.2023.168597.

[35] General Machine Timing System at GSI and FAIR.
URL https://www-acc.gsi.de/wiki/Timing/WebHome

[36] S. Jazrawi, et al., Commissioning the FAst TIMing array (FATIMA) at FAIR Phase-0: Half-lives of excited states in the $N = 50$ isotones ^{96}Pd and ^{94}Ru, Radiat. Phys. Chem. 200 (2022) 110234. doi:https://doi.org/10.1016/j.radphyschem.2022.110234.

[37] J.-M. Régis, G. Pascovici, J. Jolie, M. Rudigier, The mirror symmetric centroid difference method for picosecond lifetime measurements via Î³â€“Î³ coincidences using very fast LaBr3(Ce) scintillator detectors, Nucl. Instrum. Methods Phys. Res. A 622 (2010) 83–92. doi:https://doi.org/10.1016/j.nima.2010.07.047.

[38] J.-M. Régis, et al., The generalized centroid difference method for picosecond sensitive determination of lifetimes of nuclear excited states using large fast-timing arrays, Nucl. Instrum. Methods Phys. Res. A 726 (2013) 191–202. doi:https://doi.org/10.1016/j.nima.2013.05.126.

[39] J.-M. Régis, et al., The Generalized Centroid Difference method for lifetime measurements via $\gamma - \gamma$ coincidences using large fast-timing arrays, EPJ Web of Conferences 93 (2015) 01013. doi:https://doi.org/10.1051/epjconf/20159301013.

[40] J.-M. Régis, et al., Abrupt shape transition at neutron number $N = 60$: $B(E2)$ values in ^{94,96,98}**Sr** from fast $\gamma - \gamma$ timing, Phys. Rev. C 95 (2017) 054319. doi:https://doi.org/10.1103/PhysRevC.95.054319.

[41] D. D. Dao, F. Nowacki, Nuclear structure within a discrete nonorthogonal shell model approach: New frontiers, Phys. Rev. C 105 (2022) 054314. doi:https://doi.org/10.1103/PhysRevC.105.054314.

[42] M. Rocchini, et al., First Evidence of Axial Shape Asymmetry and Configuration Coexistence in ^{74}Zn: Suggestion for a Northern Extension of the $N = 40$ Island of Inversion, Phys. Rev. Lett. 130 (2023) 122502. doi:https://doi.org/10.1103/PhysRevLett.130.122502.

[43] G. Häfner, et al., Properties of γ-decaying isomers in the ^{100}Sn region populated in fragmentation of a ^{124}Xe beam, Phys. Rev. C 100 (2019) 024302. doi:https://doi.org/10.1103/PhysRevC.100.024302.

[44] J. Henderson, et al., Triaxiality in selenium-76, Phys. Rev. C 99 (2019) 054313. doi:https://doi.org/10.1103/PhysRevC.99.054313.

[45] H. Grawe, et al., The (6^+) isomer in 102Sn revisited: Neutron and proton effective charges close to the double shell closure, Phys. Lett. B 820 (2021) 136591. doi:https://doi.org/10.1016/j.physletb.2021.136591.

[46] R. Machleidt, High-precision, charge-dependent Bonn nucleon-nucleon potential, Phys. Rev. C 63 (2001) 024001. doi:10.1103/PhysRevC.63.024001.

[47] L. Coraggio, A. Covello, A. Gargano, N. Itaco, $g_{9/2}$ nuclei and neutron-proton interaction, Phys. Rev. C 85 (2012) 034335. doi:https://doi.org/10.1103/PhysRevC.85.034335.